Energy Advances

ROYAL SOCIETY OF CHEMISTRY

PAPER

View Article Online
View Journal | View Issue

Cite this: *Energy Adv.*, 2024, 3, 2929

Self-powered graphene-based composites for rain energy harvesting†

Yi Zheng,‡[a] Hongyu Zheng,‡[a] Yuanchong Yue,[a] Liying Lu,[b] Yingli Wang*[a] and Qunwei Tang [a]

Received 29th July 2024,
Accepted 17th September 2024

DOI: 10.1039/d4ya00479e

rsc.li/energy-advances

Harnessing waste green energy utilizing advanced energy conversion technologies is widely considered a promising avenue for enhancing the power generation capacity of renewable energy. In this study, we present the experimental realization of a tailored energy conversion device using graphene-carbon black/polyvinyl chloride (G-CB/PVC) composite films for the innovative harvesting of rainwater energy. Based on the cyclic charge–discharge behaviors of electron/cationic pseudocapacitance at the film–raindrop interface, periodic current and voltage signals were generated with maximum values exceeding 2.5 μA and 100 μV per droplet by optimizing the concentrations and species of cations, respectively. Electricity outputs were significantly enhanced by increasing the electron concentration in the composite films. It is noteworthy that rainwater energy-harvesting devices exhibit exceptional long-term stability, enduring persistent attacks posed by continuous simulated rainfall conditions.

1. Introduction

Renewable and clean energy, such as solar,[1–3] wind[4–6] and tidal[7–9] energy, has garnered widespread attention as a viable solution to the pressing issues of energy crisis and environmental pollution. Among multifarious energy-harvesting systems, photovoltaics is considered one of the most promising candidates, mainly owing to its unparalleled capability of directly converting abundant solar energy into electricity.[10–18] However, such weather-dependent devices face significant challenges in generating electricity across diverse environments. In other words, the power output yielded by a photovoltaic system can be relatively low or even zero under conditions of dim or absent light, respectively.[19–22] Statistics reveal that China enjoys an annual illumination time of approximately 3000 hours, implying that a mere 34.2% of the total illumination time can be utilized. Typically, photovoltaic power generation faces increasing challenges in regions such as Southeast Asia and South America, where rainfall is exceptionally abundant.[23] Consequently, there is an urgent need for alternative materials or innovative technologies that could meet the escalating demand for a more reliable and sustainable energy landscape based on multiple stimuli.[24]

To tackle this challenge, considerable endeavors have been devoted to yielding electricity under rainy conditions. Prior to this, our group introduced a new approach for capturing rainwater energy by leveraging reduced graphene oxide (rGO) films through a simple hot-pressing method.[25] The core operating principle underpinning this innovation primarily stems from the interaction of interfacial charges. Specifically, rainwater is inherently abundant in various ions (Na^+, Mg^{2+}, Cl^-, NO_3^-, *etc.*). Meanwhile, ample delocalized π-electrons inherent to the conjugated structure of rGO exhibit a pronounced adsorption capability towards cations present in rainwater,[26–28] forming an electric double-layer (EDL) cation/electron capacitance at rainwater–rGO interfaces. When rainwater continuously falls on the surface of rGO films, the target raindrops undergo periodic spreading/shrinking processes, ensuring repeated charging/discharging cycles, thereby persistently generating pulsing current and voltage signals.

This technology introduces a new concept for producing electricity during rainy days. Nevertheless, there are some inevitable challenges that necessitate attention: (i) the intricate and cumbersome preparation process of an indium–tin oxide (ITO) polyethylene terephthalate (PET) substrate poses a significant obstacle to the large-scale deployment of rain-powered rGO films; (ii) the reliance on large amounts of costly graphene imposes a substantial economic burden, which could potentially hinder the industrialization of the device.[29,30] To mitigate substrate costs and minimize graphene dosage, we designed a novel material that integrates high-conductivity carbon black

[a] *Institute of Carbon Neutrality, College of Chemical and Biological Engineering, Shandong University of Science and Technology, Qingdao 266590, P. R. China. E-mail: sdust2023@163.com, 18315947780@163.com, 19153733101@163.com, skdwangyingli@sdust.edu.cn, tangqunwei@sdust.edu.cn*

[b] *School of Materials Science and Engineering, Ocean University of China, Qingdao 266100, P. R. China. E-mail: 13210163509@163.com*

† Electronic supplementary information (ESI) available. See DOI: https://doi.org/10.1039/d4ya00479e

‡ Contributed equally.

with insulating polyvinyl chloride (PVC) to construct high-performance graphene-carbon black/polyvinyl chloride (G-CB/PVC) composite films.

The aforementioned species are evaluated from a multi-faceted perspective: (i) carbon black helps optimize the compatibility between graphene and PVC. (ii) Graphene, with its two-dimensional carbon layer structure adorned with abundant delocalized π-electron systems, facilitates efficient electron transport through permeation. (iii) PVC, as one of the common plastic products, finds widespread application in pipes, fittings and buildings.[31–33] Therefore, employing drainage pipes as a conduit for rainwater energy and converting it into electricity represent an ingenious strategy for achieving the efficient utilization of clean energy. The significance of this endeavor not only transcends mere electricity generation on rainy days but opens up avenues for electricity collection across various weather conditions.

2. Experimental section

2.1 Fabrication of conductive G-CB/PVC composite films

The G-CB/PVC conducting composite films were prepared as follows. Monolayer graphene nanosheets (purchased from Nanjing XFNANO Materials Tech Co., Ltd, 0.5–5 μm in size, 0.8–1.2 nm in thickness) and carbon black powders (purchased from Aladdin Bio-Chem Technology Co., Ltd, 100–200 μm in size, 280 g L^{-1} in density) with mass ratio of 6 : 1 were dispersed in 2 wt% ethanol aqueous solution and subsequently treated ultrasonically for 1 hour under sealed condition at room temperature. Another solution including 0.1 g of powdered PVC was added in 20 mL of tetrahydrofuran, which was completely dissolved by ultrasonication at room temperature for 3 hours. Subsequently, the two aforementioned solutions were meticulously combined and sealed within an ultrasonic environment for 2 hours, facilitating the formation of a homogenous dispersion. This blended dispersion was then carefully coated onto a 4 × 5 cm^2 substrate, which could encompass a variety of materials such as plastic, glass, and tile. The coated substrate was allowed to dry naturally in air, resulting in the production of the conductive G-CB/PVC composite films with a total thickness of 65 ± 10 μm.

2.2 Device assembly and measurements

The rain-responsive device was crafted with a "sandwiching" architecture comprising collectors, film and substrate. The dual copper-based collectors were covered by silver paint and further enveloped in a protective sheath of ethylene vinyl acetate copolymer. A medical syringe filled with ionic solution was adopted to simulate the rainfall process by controlling the injection velocity. The tilted angle of the film and distance between the tip and film were 30° and 30 mm, respectively. The raindrops were injected onto the surface of conductive G-CB/PVC composite films; meanwhile, the electrical signals were recorded by two collectors. In this fashion, the *i*–*t* curve (sample interval: 0.05 s) and *v*–*t* curve (sample interval: 0.1 s) were tested to evaluate the current and voltage values, respectively, using approximately linear baselines as benchmarks generated by the deionized aqueous solution. Furthermore, the linear *I*–*V* curves were obtained utilizing an electrochemical workstation (CHI660E) interfaced with two collecting electrodes. These linear *I*–*V* profiles (sample interval: 0.001 V) before and after dropping the simulated rainwater were generated in the scan ranging from −1.0 to 1.0 V executed at a rate of 100 mV s^{-1} to demonstrate the change in ohmic resistances. In this work, 0.6 M NaCl aqueous solution was

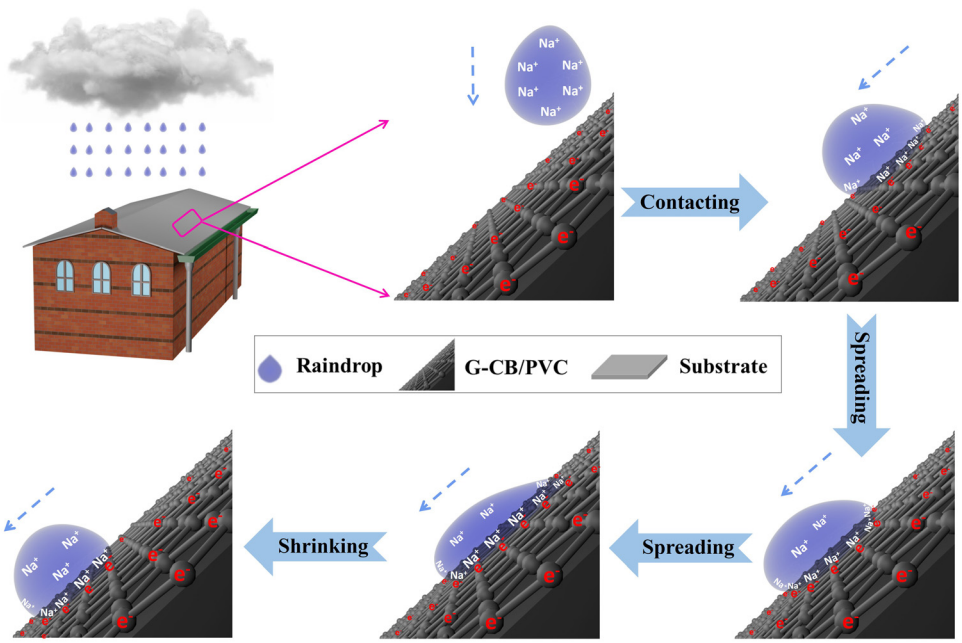

Fig. 1 Schematic of the working mechanism for rain-enabled G-CB/PVC composite films in electricity outputs.

consistently applied as the simulated rainwater unless mentioned otherwise.

2.3 Electrochemical characterization

A symmetric dummy cell with 94 wt% G-CB/PVC film|0.6 M NaCl|94 wt% G-CB/PVC film architecture was prepared for cycle voltammetry (CV) and electrochemical impedance spectroscopy (EIS) characterization. The CV curves were recorded by scanning from 0 to +0.3 V and back to 0 V. The capacitance was calculated using the equation $C = S/(\nu \times \Delta V)$, where C represents capacitance, S represents the area within the CV curve, ν represents the scan rate (20 mV s^{-1}), and ΔV represents the potential span for the CV test (0.3 V). The EIS plots were also measured on the symmetric dummy cell in the frequency range from 0.1 to 1×10^5 Hz with an amplitude of 5 mV. The contact angle was measured utilizing SDC-350KS, and the angle test method was applied to fit the Young–Laplace equation.

3. Results and discussion

The structure and working mechanism of rain-triggered conductive films for energy harvesting are illustrated in Fig. 1. The device integrates the G-CB/PVC composite films, anchored onto a durable glass substrate, with dual silver-coated copper electrodes functioning as the collecting electrodes. Upon the impact of simulated raindrops on the surface of G-CB/PVC composite films, the droplets rapidly disperse towards the perimeter. Specifically, the cations in the raindrops, such as Na^+, engage in electrostatic attraction with the π-electrons from the conductive materials, causing their adsorption. Subsequently, the migration of the target π-electrons generates electrical signals that mirror the charging behavior. As the raindrops undergo evaporation and shrink, the cations are released from the rear end of the droplet, freeing the working π-electrons back onto the G-CB/PVC films. This reversal constitutes a discharging process, accompanied by a decrease in

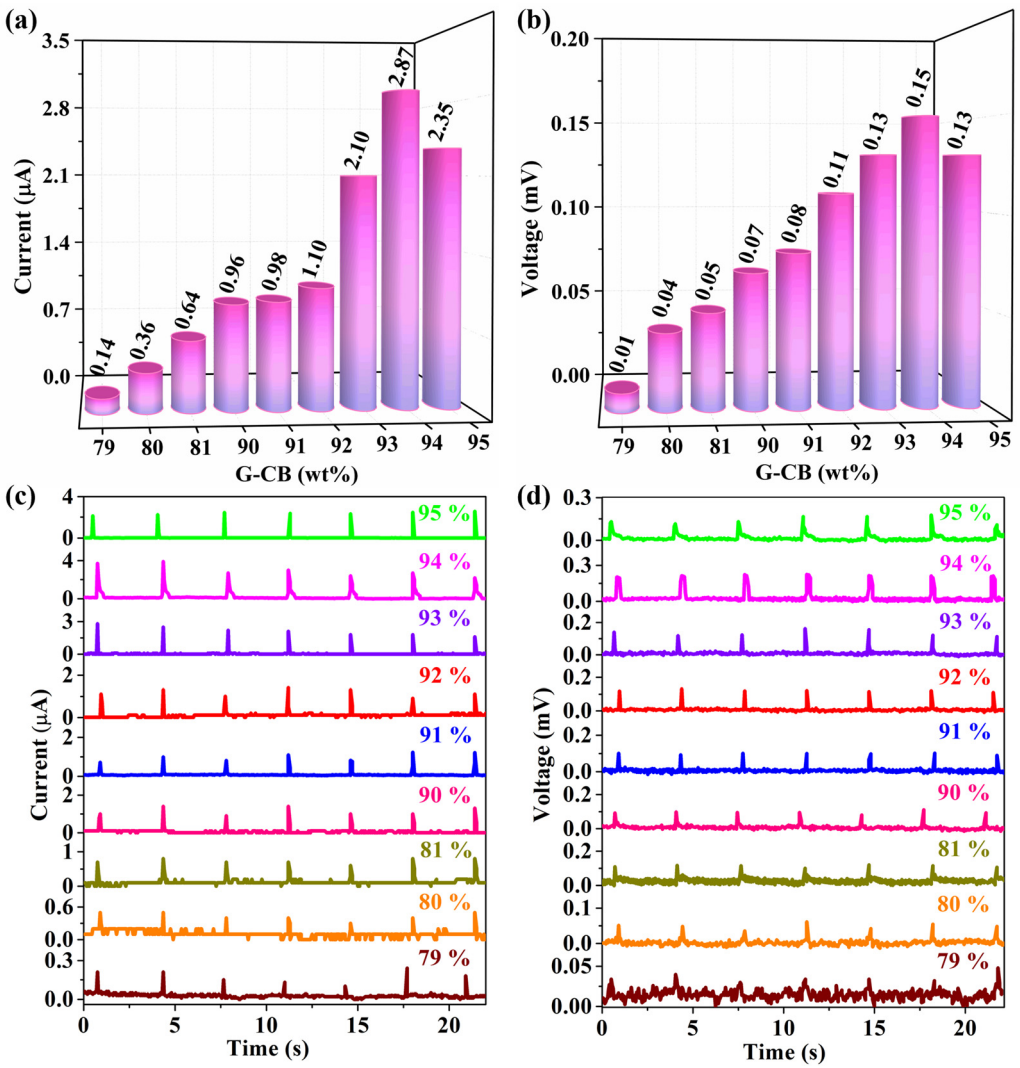

Fig. 2 Histograms of (a) current and (b) voltage values by dropping 0.6 M NaCl aqueous solution on G-CB/PVC composite films at various G-CB dosages. (c) Current and (d) voltage signals. The injection velocity is 60 mL h^{-1}.

signal intensity. Harnessing the charging and discharging mechanisms inherent to the cation (from rainwater)/electron (derived from the G-CB/PVC film) EDL capacitances at the rain–film interface, periodical electrical signals are yielded under the stimulation of raindrops. Notably, the peak signal amplitudes serve as quantitative indicators, enabling the assessment of the device's performance in converting rainwater energy into usable electricity.

Furthermore, the contact angles of 0.6 M NaCl droplet (Fig. S1(a), ESI†) and pure water (Fig. S1(b), ESI†) dropped onto the 94 wt% G-CB/PVC film were measured to characterize the differences in wettability. It can be visually observed that the contact angle of the 0.6 M NaCl droplet (80.77°) is smaller than that of pure water (106.04°), indicating a partial hydrophobic nature of the G-CB/PVC film. This result validates that the cations within the droplets can be absorbed and desorbed during the spreading and shrinking processes because of the partial hydrophobic surface of the G-CB/PVC, thereby suggesting the dependence of the electrical signals on the time interval.

Fig. 2 delves into the influence of G-CB/PVC composite films incorporating varying G-CB dosages on the electrical signals, with the pivotal findings summarized in Table 1. The conductive nature of these G-CB/PVC films is evidenced by the periodic capture of current and voltage fluctuations within the G-CB dosage range of 79–95 wt%, demonstrating their potential to generate electrical signals at the interface with rainwater and G-CB/PVC composite films.[34] Notably, a stark contrast emerges between the subdued signal intensities observed at G-CB dosages below 20 wt% and the marked augmentation in both current and voltage when the dosage escalates to 94 wt%. Precisely, the current increases to 2.87 ± 0.70 μA and the voltage reaches 0.15 ± 0.04 mV at the optimal 94 wt% G-CB dosage. With further increments in dosage, the corresponding electrical signals decline slightly, which is possibly attributable to the deterioration of the mechanical properties of the G-CB/PVC film due to the random and uneven distribution of G-CB dosage. Consequently, a refined G-CB dosage of 94 wt% was deemed optimal for subsequent experiments.

Table 1 Electrical data produced by 0.6 M NaCl aqueous solution on G-CB/PVC composite films at various G-CB dosages at an injection velocity of 60 mL h^{-1}

G-CB dosage (wt%)	Current (μA)	Voltage (mV)
79	0.14 ± 0.11	0.01 ± 0.01
80	0.36 ± 0.06	0.04 ± 0.01
81	0.64 ± 0.06	0.05 ± 0.01
90	0.96 ± 0.04	0.07 ± 0.10
91	0.98 ± 0.14	0.08 ± 0.18
92	1.10 ± 0.20	0.11 ± 0.01
93	2.10 ± 0.70	0.13 ± 0.03
94	2.87 ± 0.70	0.15 ± 0.04
95	2.35 ± 0.22	0.13 ± 0.05

As mentioned before, the manifestation of percolating behavior assumes paramount significance in evaluating the conductivity characteristics of G-CB/PVC films.[35] Fig. 3 elucidates the dependence of electrical signal on the varying dosage of G-CB, where both current and voltage values exhibit similar percolating tendency with a percolation threshold at 94 wt% G-CB species. This phenomenon is linked to the formation of interconnected channels that facilitate the efficient transportation of π-electrons during the electricity-generation process. Hence, this affirms that G-CB/PVC composite films possess immense potential for harvesting rain energy.

The intriguing phenomenon whereby simulated raindrops generate electric signals upon impact on composite films can be quantified utilizing ohmic resistance. As a reference, 94 wt% G-CB/PVC film with and without 0.6 M NaCl aqueous solution was tested, as shown in Fig. S2(a) (ESI†). The resistance values derived from the linear *I*–*V* curves are almost identical before and after dropping rainwater, underscoring that the pulsed peaks reflect real electrical signals free of ohmic fluctuations. Furthermore, as depicted in Fig. S2(b) (ESI†), deionized water was substituted for the 0.6 M NaCl aqueous solution in this experiment. As a result, neither current nor voltage was detected, suggesting that ions in rainwater serve as a pivotal factor in yielding electricity. This finding underscores the critical role of ions in facilitating the intriguing electrical response elicited by simulated rainfall on these composite films.

As is well known, rainfall intensity exhibits significant variability around the world. A medical syringe imbued with

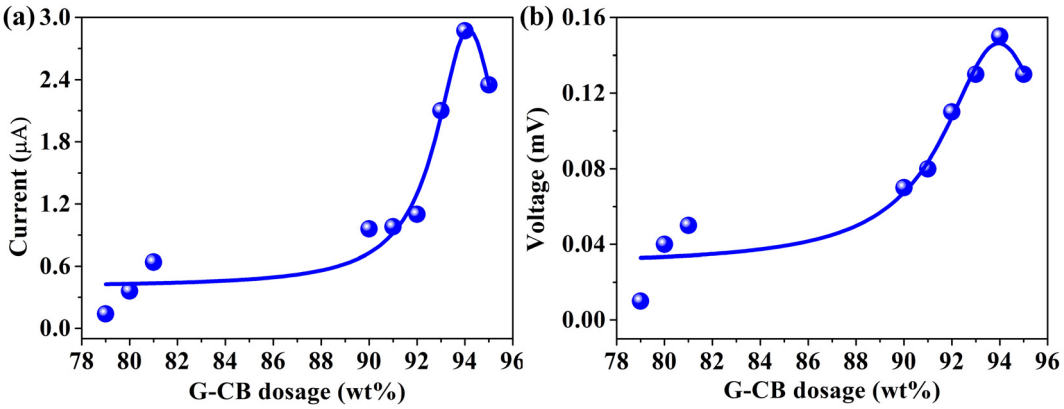

Fig. 3 The plots of (a) current and (b) voltage as a function of G-CB dosage.

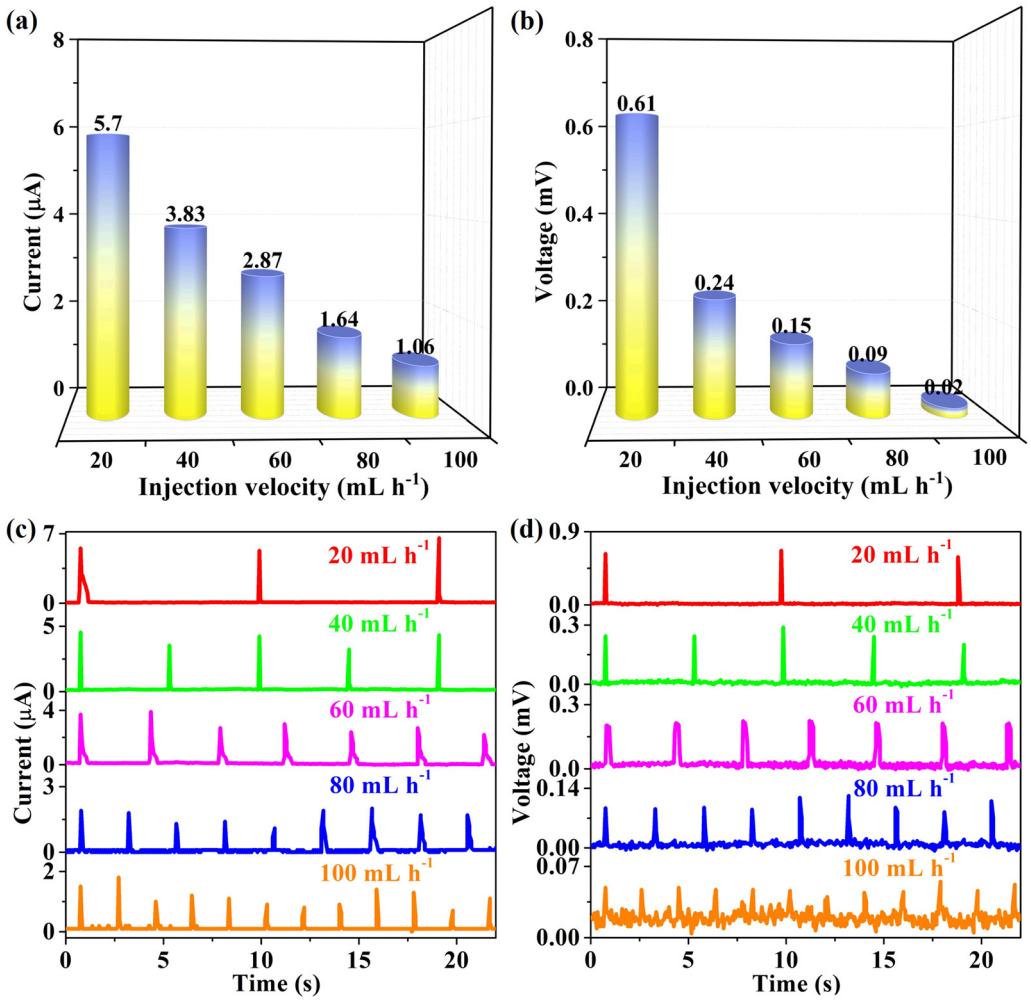

Fig. 4 Histograms of (a) current and (b) voltage values by dropping 0.6 M NaCl aqueous solution on the 94 wt% G-CB/PVC composite film at different intervals of two droplets by controlling the injection velocities. (c) Current and (d) voltage signals.

ionic solution was employed with different injection velocities meticulously manipulated to simulate the natural occurrence of raindrops. By adjusting the injection rate within the range from 100 to 20 mL h^{-1}, the electrical signals were captured and analyzed by an electrochemical workstation (CHI660E); the generated electrical signals are depicted in Fig. 4, while the corresponding data are meticulously tabulated in Table 2. The corresponding signal outputs exhibit a pronounced increase, with the current ranging from 1.06 ± 0.46 μA to 5.70 ± 0.97 μA for current and voltage escalating from 0.02 ± 0.01 mV to 0.61 ± 0.02 mV, respectively. This substantial variation demonstrates the remarkable capacity of rain-triggered G-CB/PVC composite films to generate electricity. Furthermore, it is crucial to acknowledge that the power-generation potential is related to the interval time between two adjacent raindrops. With an increase in rainfall intensity, the observed electrical signals decrease. A plausible explanation is that the active raindrops generate partial spreading/shrinking processes accompanied by incomplete charging and discharging cycles. Hence, the conductive 94 wt% G-CB/PVC composite film emerges as an ideal choice for regions characterized by light rainfall. Unless otherwise specified, a moderate injection velocity of 60 mL h^{-1} was adopted in our experiment, providing a consistent basis for comparison and analysis.

Table 2 Electrical data produced by 0.6 M NaCl aqueous solution on 94 wt% G-CB/PVC composite films at various injection velocities

Injection velocity (mL h^{-1})	Current (μA)	Voltage (mV)
20	5.70 ± 0.97	0.61 ± 0.02
40	3.83 ± 0.79	0.24 ± 0.04
60	2.87 ± 0.70	0.15 ± 0.04
80	1.64 ± 0.54	0.09 ± 0.02
100	1.06 ± 0.46	0.02 ± 0.01

The charging and discharging reactions underlying the EDL (electric double layer) capacitance behavior can be probed more thoroughly through cyclic voltammogram (CV) analyses employing custom-built symmetric dummy cells comprising a 94 wt% G-CB/PVC film 0.6 M NaCl electrolyte 94 wt% G-CB/PVC film configuration. As illustrated in Fig. 5(a), the capacitance

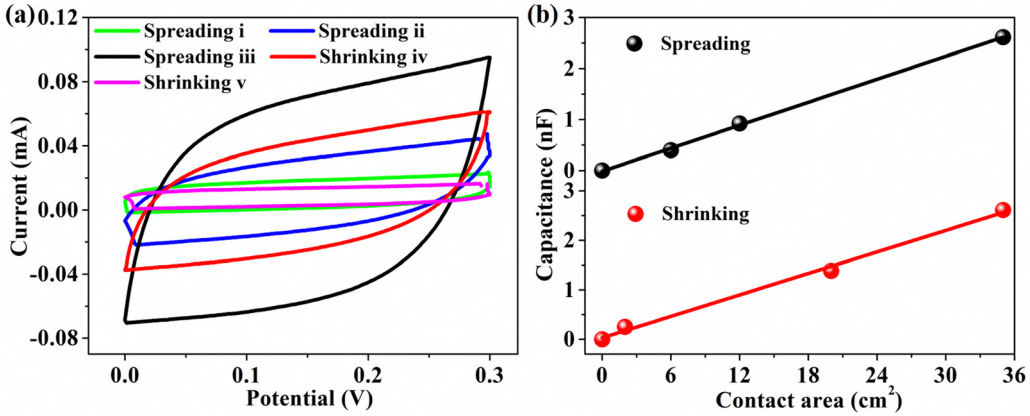

Fig. 5 (a) CV curves for the symmetric dummy cells with 94 wt% G-CB/PVC film 0.6 M NaCl 94 wt% G-CB/PVC film architecture. (b) Linear plots of the capacitance as a function of the contact area between a raindrop and the 94 wt% G-CB/PVC composite film.

dynamics during swift charging and discharging cycles are manifested as rectangular-like CV profiles, showcasing a capacitance range spanning from 0 pF under raindrop-free conditions to a peak of 2612 pF when raindrops are maximally spread (refer to Table S1 for details, ESI†). Notably, upon raindrop shrinkage, this capacitance value correspondingly dwindles back to 0 pF. Additionally, the expansion and contraction of the capacitive response exhibit a linear correlation with the varying contact area interface between the raindrops and the 94 wt% G-CB/PVC film, as evident in Fig. 5(b),

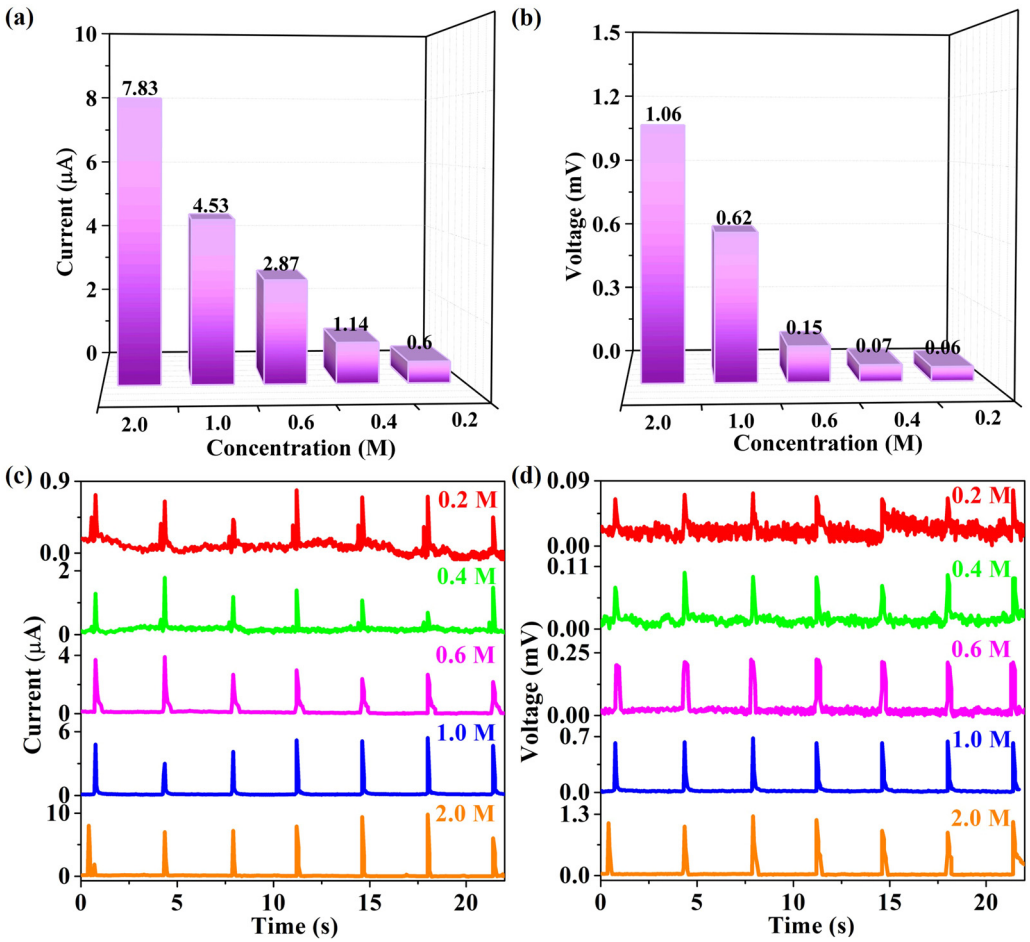

Fig. 6 Histogram of (a) current and (b) voltage values by dropping NaCl aqueous solution with different concentrations on the 94 wt% G-CB/PVC film at an injection velocity of 60 mL h^{-1}. (c) Current and (d) voltage signals.

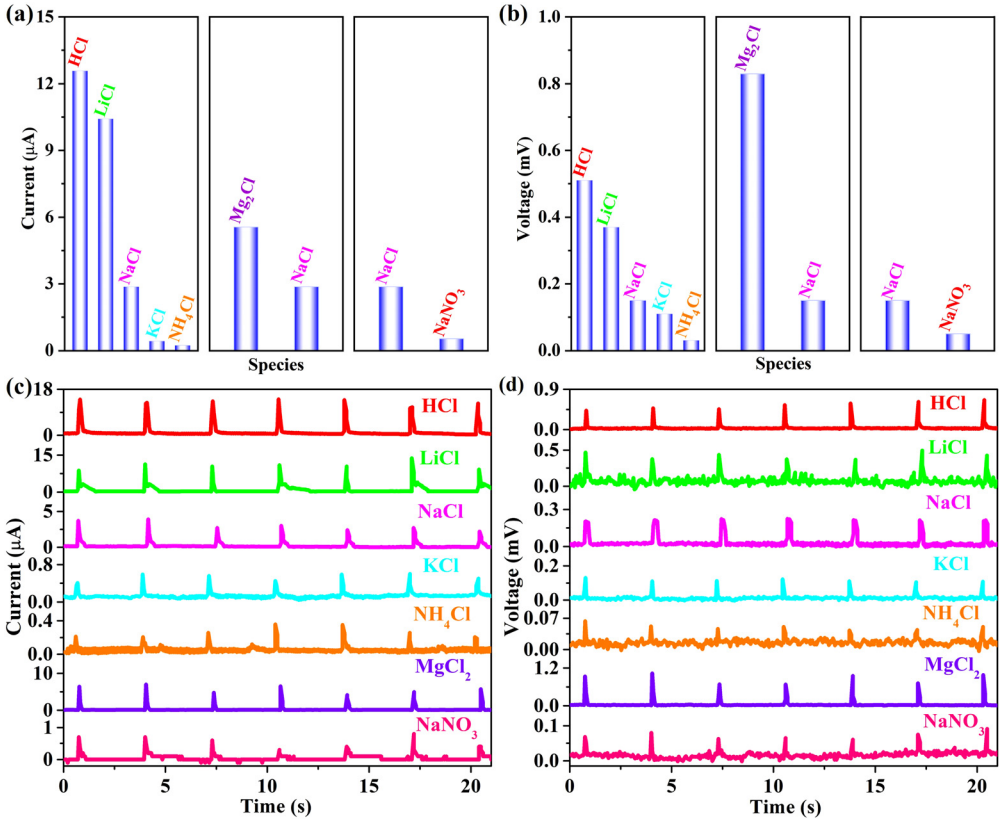

Fig. 7 Histograms of (a) current and (b) voltage values by dropping 0.6 M chlorides and $NaNO_3$ aqueous solution on the 94 wt% G-CB/PVC film at an injection velocity of 60 mL h^{-1}. (c) Current and (d) voltage signals.

underscoring the sensitivity of the system to these dynamic interfacial changes.

Additionally, electrochemical impedance spectroscopy (EIS) was implemented to elucidate the intricate mechanism of charge adsorption and transportation. An equivalent circuit could be extracted by fitting the EIS diagram (depicted in Fig. S3(a), ESI†) with Z-view software, and the pertinent electrochemical parameters are summarized in Fig. S3(b) and Table S1 (ESI†). The contact resistance (R_s) can be formed once the simulated raindrops fall onto the G-CB/PVC composite film, facilitating the subsequent adsorption of cation by the abundant delocalized π-electrons inherent in graphene. This interaction triggers the formation of an electron/cationic EDL, thereby producing capacitance CPE. Moreover, the dynamic processes of positive charge diffusion and contraction within the system are accompanied by the manifestation of two distinct resistances, namely, the charge-transfer resistance (R_{ct}) and the Warburg impedance (W), which reflect the intricacies of these charge movement phenomena.

The aforementioned investigations have proved the pivotal influence of ions on the signal values, thereby necessitating a deeper exploration into the impact of ionic concentration on power generation. In this regard, the concentrations of aqueous solution are tagged as 0.2, 0.4, 0.6, 1.0 and 2.0 M, respectively. As displayed in Fig. 6 and Table S2 (ESI†), each signal value adheres to the order $NaCl_{(2.0M)}$ > $NaCl_{(1.0M)}$ > $NaCl_{(0.6M)}$ > $NaCl_{(0.4M)}$ > $NaCl_{(0.2M)}$. Apparently, both current and voltage are gradually enhanced with increasing concentration, benefiting from the improved EDL capacitance at the interface between rainwater and the 94 wt% G-CB/PVC film. Thus, this rain-activated film holds immense promise for application in coastal regions.

Based on the fundamental premise of rain-responsive G-CB/PVC composite films, ionic species also emerge as pivotal factors influencing their electricity-yielding capacity. As exhibited in Fig. 7, a comprehensive analysis was conducted on a 0.6 M chloride aqueous solution encompassing HCl, LiCl, NaCl, KCl, NH_4Cl and $MgCl_2$ with the consolidated outcomes tabulated in Table 3. The electrical responses derived from the 94 wt% G-CB/PVC material follow the order HCl > LiCl > NaCl >

Table 3 Histograms of electric signals by dropping 0.6 M chlorides and $NaNO_3$ aqueous solution on 94 wt% G-CB/PVC films at an injection velocity of 60 mL h^{-1}

Chlorides	Current (μA)	Voltage (mV)
HCl	12.57 ± 0.73	0.51 ± 0.08
LiCl	10.42 ± 1.46	0.37 ± 0.10
NaCl	2.87 ± 0.70	0.15 ± 0.04
KCl	0.42 ± 0.06	0.11 ± 0.01
NH_4Cl	0.24 ± 0.08	0.03 ± 0.02
$MgCl_2$	5.56 ± 1.50	0.83 ± 0.18
$NaNO_3$	0.53 ± 0.27	0.05 ± 0.04

KCl > NH_4Cl. This behavior can be rationalized through Coulomb's effect, manifesting in the descending order of ionic radius: [$r(H^+)$ = 32 pm] < [$r(Li^+)$ = 60 pm] < [$r(Na^+)$ = 95 pm] < [$r(K^+)$ = 122 pm] < [$r(NH_4^+)$ = 133 pm]. As the ionic radius diminishes, an intensified electrostatic interaction ensues between the cations and electrons, fostering a heightened electron/cation EDL capacitance. This result confirms the promising potential of conductive G-CB/PVC composites for harvesting rainwater energy. Illustrating with the current as a case in point, it becomes evident that the HCl aqueous solution yields the most pronounced signal (12.57 ± 0.73 μA), surpassing those from other chloride solutions (LiCl: 10.42 ± 1.46 μA, NaCl: 2.87 ± 0.70 μA, KCl: 0.42 ± 0.06 μA, NH_4Cl: 0.24 ± 0.08 μA), positioning it as a promising candidate for application in acid-rain environments.

The report meticulously reveals that both Hofmeister effect and electrostatic interactions collaborate to significantly amplify the ionic conductivity of organohydrogels.[36] Notably, the electrostatic interplay between lithium and sodium bonds emerges as the paramount factor, surpassing the Hofmeister effect in its contribution to enhancing the conductivity. This observation holds potential relevance to our research endeavors, where the electrostatic forces between cations (Li^+, Na^+, K^+, *etc.*) and electrons dominate over the Hofmeister effect. Furthermore, the electrostatic interactions adhere to a distinct hierarchy of $Li^+ > Na^+ > K^+$, implying that the electrical signal transmission efficiency follows a similar trend, with LiCl outperforming NaCl, which in turn surpasses KCl.

Furthermore, when $MgCl_2$ solution is employed as simulated rainwater, both current and voltage levels exhibit an upsurge compared to NaCl, which is attributed to the radius of Mg^{2+} (67 pm) being lower than that of Na^+ (95 pm), coupled with its higher charge valence. The Hofmeister series of Mg^{2+} exhibits a likeness to that of Li^+, yet with a distinct advantage as Mg^{2+} carries two charges compared to the single charge of Li^+. Consequently, Mg^{2+}, boasting two transferable electrons, manifests a superior volume density compared to Li^+.

Besides, anions derived from rainfall, such as Cl^- and NO_3^-, also play a pivotal role in modulating the electrical signals. With the anion as a signal variable (NaCl and $NaNO_3$), the associated electricity outputs of the former exhibit an increasing, even three-time higher, value than that of the latter. Due to a larger ionic radius and further a weaker adsorption capacity of Cl^- than that of NO_3^-, the electrostatic adsorption force with Na^+ becomes stronger.

Crucially, long-term stability is regarded as a cornerstone prerequisite for evaluating the viability of implementation in actual operations. As a result, the stabilities of both current and voltage generated from the 94 wt% G-CB/PVC film over 1000 s were recorded and are shown in Fig. 8. Despite a slight fluctuation in the baseline of either current or voltage, the overall electrical signals remain relatively stable. In general, this device provides guidance for the development of the power market. The attenuation of the active signals can be deduced through a few plausible explanations. Firstly, the inherent hydrophobicity of the G-CB/PVC film surface fosters an elevation in the

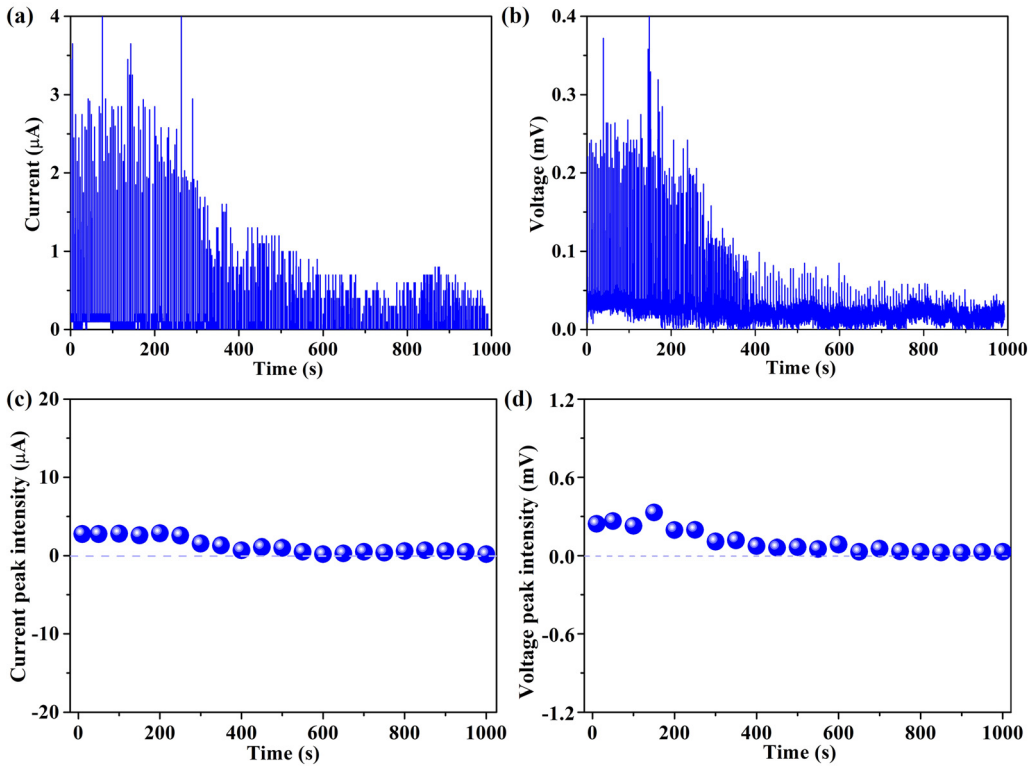

Fig. 8 Stability of (a) current and (b) voltage by persistently dropping 0.6 M NaCl aqueous solution on the 94 wt% G-CB/PVC film at an injection velocity of 60 mL h^{-1}. The durability of (c) current and (d) voltage outputs.

contact resistance between the simulated rainwater and film. It is difficult for the conductive film to be hydrated or infiltrated, which results in some ions having no chance to combine with the electrons and therefore being incapacitated in generating electricity. Additionally, with the vast and rapid raindrops falling, the previously occupied electrons cannot be duly released or undergo further adsorption/desorption dynamic with the incoming ions.

All aforementioned electricity performance evaluations to date have been conducted utilizing simulated rainwater conditions. To mirror the practical application of this device in actual rainfall environments, real rainwater from Qingdao, China was collected to determine the electrochemical performances. The optimized 94 wt% G-CB/PVC film was employed and periodic signal peaks were collected at an injection velocity of 40 mL h^{-1}. As depicted in Fig. S4 and Table S3 (ESI†), the current, voltage and power values were 0.59 μA per drop, 38.82 μV per drop and 30.90 pW per drop, respectively. The electrical outputs appear modest due to the inherently low ion concentration, while a promising solution for real application lies in deploying large-scale 94 wt% G-CB/PVC composite electrodes to concurrently harness rain energy. This finding underscores the potential of these film-based rain energy converters crafted from conductive G-CB/PVC film as viable candidates for practical rain energy-harvesting applications.

4. Conclusions

In summary, we demonstrated that the rain-enabled G-CB/PVC composite film paired with delocalized enriched-electron systems significantly enhances the energy-harvesting capabilities in rainy conditions. Attributed to the cycling charging/discharging EDL capacitances at the raindrop–film interface, periodic electrical signals including current and voltage can be generated in tens to thousands of micron levels. Because of the widespread applications of PVC materials in buildings, sewers and other fields, the emergence of these conductive G-CB/PVC composite films holds immense promise for generating electricity in daily life. Although the endeavors in the current study are in their nascent stages, there is immense potential for ground-breaking advancements through fundamental research and technological innovations aimed at cost reduction. Notably, the development of rain-powered energy generation platforms may inspire scientists to delve into sophisticated energy harvesting devices tailored for environments characterized by abundant rainfall, acid rain and offshore navigation scenarios.

Author contributions

Yingli Wang and Qunwei Tang conceptualized the project; Yi Zheng, Hongyu Zheng performed the experiment; Yi Zheng, Hongyu Zheng, Yuanchong Yue and Liying Lu analyzed the data; Yingli Wang wrote the manuscript.

Data availability

The authors confirm that the data supporting the findings of this study are available within the article and its ESI.†

Conflicts of interest

There are no conflicts to declare.

Acknowledgements

This work was supported by National Key Research and Development Program of China (2021 YFE0111000), the National Natural Science Foundation of China (22309107), Natural Science Foundation of Shandong Province, China (ZR2023QB281).

References

1 W.-H. Chen and F. Q. You, *Appl. Energy*, 2024, **372**, 123802.
2 B. Yang, C. Y. Li, Z. F. Wang and Q. Dai, *Adv. Mater.*, 2022, **34**, 2107351.
3 J. H. Jin, Q. Wang, K. G. Ma, W. F. Shen, L. A. Belfiore, X. C. Bao and J. G. Tang, *Adv. Funct. Mater.*, 2023, **33**, 2213324.
4 O. Ozkan, M. N. Coban and M. A. Destek, *Renewable Energy*, 2024, **228**, 120623.
5 Z. W. Ren, L. T. Wu, Y. K. Pang, W. Q. Zhang and R. S. Yang, *Nano Energy*, 2022, **100**, 107522.
6 X. Zhao, A. Nashalian, I. W. Ock, S. Popoli, J. Xu, J. Y. Yin, T. Tat, A. Libanori, G. R. Chen, Y. H. Zhou and J. Chen, *Adv. Mater.*, 2022, **34**, 2204238.
7 D. Khojasteh, M. Lewis, S. Tavakoli, M. Farzadkhoo, S. Felder, G. Lglesias and W. Glamore, *Renewable Sustainable Energy Rev.*, 2022, **156**, 111855.
8 L. Perez, R. Cossu, A. Grinham and I. Penesis, *Renewable Energy*, 2021, **178**, 1322–1336.
9 C. X. Mo, W. Q. Zhu, B. Q. Lu, S. Zu, F. L. Zhang, J. M. Chen, X. Zhang, B. G. Wu, X. M. Zhang and J. P. Huang, *Energy*, 2024, **302**, 131799.
10 Y. X. Li, X. J. Huang, H. K. M. Sheriff Jr and S. R. Forrest, *Nat. Rev. Mater.*, 2023, **8**, 186–201.
11 R. A. M. Lameirinhas, J. P. N. Torres and J. P. de Melo Cunha, *Energies*, 2022, **15**, 1823.
12 S. Zhang, Z. K. Liu, X. T. Zhang, Z. H. Wu and Z. Y. Hu, *Innovation*, 2024, **5**, 100591.
13 M. Moser, A. Wadsworth, N. Gasparini and L. McCulloch, *Adv. Energy Mater.*, 2021, **11**, 2100056.
14 D. Singh, R. Chaudhary and A. Karthick, *Environ. Sci. Pollut. Res.*, 2021, **28**, 47689–47724.
15 S. Ghosh and R. Yadav, *Sustainable Energy Technol.*, 2021, **47**, 101410.
16 V. Pecunia, L. G. Occhipinti and R. L. Z. Hoye, *Adv. Energy Mater.*, 2021, **11**, 2100698.
17 P. Chatterjee, M. S. K. Ambati, A. K. Chakraborty, S. Chakrabortty, S. Biring, S. Ramakrishna, T. K. S. Wong, A. Kumar, R. Lawaniya and G. K. Dalapati, *Energy Convers. Manage.*, 2022, **261**, 115648.

18 Y. G. Landera, O. C. Zevallos, R. C. Neto, J. F. da, C. Castro and F. A. S. Neves, *Energies*, 2023, **16**, 2093.
19 H. Kanda, V. D. Mihailetchi, M.-E. Gueunier-Farret, J.-P. Kleider, Z. Djebbour, J. Alvarez, B. Philippe, O. Isabella, M. R. Vogt, R. Santbergen, P. Schulz, F. Peter, M. K. Nazeeruddin and J. P. Connolly, *Interdiscip. Mater.*, 2022, **1**, 148–156.
20 R. Steim, T. Ameri, P. Schilinsky, C. Waldauf, G. Dennler, M. Scharber and C. J. Brabec, *Sol. Energy Mater. Sol. Cells*, 2011, **95**, 3256–3261.
21 L. Xie, W. Song, J. F. Ge, B. Tang, X. L. Zhang, T. Wu and Z. Y. Ge, *Nano Energy*, 2021, **82**, 105770.
22 N. Rathore, N. L. Panwar, F. Yettou and A. Gama, *Int. J. Ambient Energy*, 2021, **42**, 1200–1217.
23 Y. W. Wang, Y. C. Wei, K. C. Li, X. T. Jiang, C. L. Li, Q. Y. Yue, B. C.-Y. Zee and K. C. Chong, *Environ. Int.*, 2022, **169**, 107518.
24 Z. T. Li, X. T. Xu, X. R. Sheng, P. Lin, J. Tang, L. K. Pan, Y. V. Kaneti, T. Yang and Y. Yamauchi, *ACS Nano*, 2021, **15**, 12535–12566.
25 Q. W. Tang, X. P. Wang, P. Z. Yang and B. L. He, *Angew. Chem., Int. Ed.*, 2016, **55**, 5243–5246.
26 S. F. Wang, P. Sun, N. Li, J. G. Wang, L. Zhang, W. J. Duan and Z. F. Li, *J. Power Sources*, 2023, **556**, 232471.
27 N. Dimov, A. Staykov, M. I. M. Kusdhany and S. M. Lyth, *Nanotechnology*, 2023, **34**, 415001.
28 T. Wang, S. Sanz, J. Castro-Esteban, J. Lawrence, A. Berdonces-Layunta, M. S. G. Mohammed, M. Vilas-Varela, M. Corso, D. Peña, T. Frederiksen and D. G. de Oteyza, *Nano Lett.*, 2022, **22**, 164–171.
29 P. Aiswaria, S. N. Mohamed, D. L. Singaravelu, K. Brindhadevi and A. Pugazhendhi, *Chemosphere*, 2022, **296**, 133983.
30 M. Hosseinnezhad, M. Ghahari, G. Mobarhan, S. Rouhani and M. Fathi, *Opt. Mater.*, 2023, **139**, 113775.
31 P. Lieberzeit, D. Bekchanov and M. Mukhamediev, *Polym. Adv. Technol.*, 2022, **33**, 1809–1820.
32 Z. Zhang, H. R. Peng, D. C. Yang, G. Q. Zhang, J. L. Zhang and F. Ju, *Nat. Commun.*, 2022, **13**, 5360.
33 Y. M. Sun, H. L. Liu, Y. Qin, X. S. Feng, J. Y. Chen, Q. L. Huang and C. F. Xiao, *Sep. Purif. Technol.*, 2023, **317**, 123831.
34 J. Yin, X. M. Li, J. Yu, Z. H. Zhang, J. X. Zhou and W. L. Guo, *Nat. Nanotechnol.*, 2014, **9**, 378–383.
35 O. Trotsenko, A. Tokarev, A. Gruzd, T. Enright and S. Minko, *Nanoscale*, 2015, **7**, 7155–7161.
36 Y. Wu, Y. Mu, Y. Luo, C. Menon, Z. Zhou, P. Chu and S.-P. Feng, *Adv. Funct. Mater.*, 2022, **32**, 2110859.